

Coherent modes of X-ray beams emitted by undulators in new storage rings

Mark Glass and Manuel Sanchez del Rio
ESRF - The European Synchrotron
 71, Avenue des Martyrs, Grenoble, France
 (Dated: July 13, 2021)

Synchrotron radiation emitted by electrons passing through an undulator placed in a storage ring is decomposed in coherent modes. The case of ultimate storage rings where the electron emittance is comparable to the emittance of the photon fan is analyzed by means of the cross spectral density and the coherent mode spectrum. The proposed method permits naturally the statistical analysis and propagation of the cross spectral density along the beamline optics. The coherence properties of the X-ray beam at any point of the beamline are completely given in terms of the eigenvalues and coherent modes of the cross spectral density.

Synchrotron radiation (SR) has witnessed an enormous growth in the last decades because of its applicability to multidisciplinary applied science. Several generations of synchrotron radiation sources (first generation or application of SR in parasitic mode, second generation or storage rings dedicated to SR, third generation or storage rings with long straight sections to hold undulators) have raised the brilliance with rates even higher than the Moore law. The current third generation of synchrotrons is now continued in two different new facilities: X-ray free electron lasers (XFELs), based on linear accelerator technology, and the so-called “diffraction limited storage rings”. These are circular storage rings where the electron horizontal emittance is lowered to a level comparable to the present vertical emittance, which is small enough to allow experiments exploiting the X-ray beam coherence. In this context, many experimental techniques have developed, like X-ray photon correlation spectroscopy, coherent diffraction imaging, or ptychography. In all new facilities or upgrades of the existing ones, the keyword “coherence” is omnipresent. We look to the upgrade of the existing facilities, like the EBS (Extremely Brilliant Source) at the European Synchrotron Radiation Facility, aiming at building a storage ring of 150 pm emittance (as compared with the present one of 4 nm) that will boost the X-ray brilliance and the coherence properties. The accurate calculation and quantitative evaluation of the parameters related to X-ray coherence in new storage rings is the subject of this paper.

The calculation of observable quantities of the emission like the mean intensity requires a statistical approach. Kim [1] proposed a method to calculate the Wigner functions of synchrotron undulators for many practical cases. The method was revisited by Geloni *et al.* in a rigorous statistical optics context [2]. One may define a virtual source in a plane before the beamline with the property that an electric field propagated from the virtual source to a position along the beamline reproduces the real electric field at that position. For sufficiently long electron beam bunches the storage ring emission can be considered wide-sense stationary for many practical applications [2]. We can therefore describe second order co-

herence phenomena in frequency domain with the cross spectral density (CSD) $W(\mathbf{r}_1, \mathbf{r}_2, \omega)$ where $\mathbf{r}_1, \mathbf{r}_2$ are spatial coordinates and ω is the radiation frequency. If additionally the variation of the undulator magnetic field is negligible along the electron beam dimension, the cross spectral density at the virtual source is given by:

$$W(\mathbf{r}_1, \mathbf{r}_2, \omega) = N_e \int d\gamma d\mathbf{r} d\boldsymbol{\theta} \rho(\mathbf{r}, \boldsymbol{\theta}, \gamma) e^{ik\boldsymbol{\theta}(\mathbf{r}_2 - \mathbf{r}_1)} \times E_0^*(\gamma, \mathbf{r}_1 - \mathbf{r}, \omega) E_0(\gamma, \mathbf{r}_2 - \mathbf{r}, \omega) \quad (1)$$

where N_e is the number of electrons, ρ is the five-dimensional spatial, angular and energy dependent electron phase space distribution, E_0 is the reference electric field created by a reference electron, the star denotes complex conjugation and γ is the relativistic Lorentz factor of the electrons. The exact reference electric field E_0 produced by an undulator is given by [3]:

$$\mathbf{E}(\mathbf{R}, \omega) = \frac{i e \omega}{4 \pi c \epsilon_0} \times \int \left[\frac{\mathbf{n} \times [(\mathbf{n} - \dot{\mathbf{r}}) \times \dot{\mathbf{r}}]}{(1 - \dot{\mathbf{r}}\mathbf{n})^2} + \frac{c}{\gamma^2 R} \frac{(\mathbf{n} - \dot{\mathbf{r}})}{(1 - \dot{\mathbf{r}}\mathbf{n})^2} \right] e^{i\omega(t - \mathbf{n}\mathbf{r}(t)/c)} dt \quad (2)$$

where e is the electron charge, c the velocity of light, ϵ_0 the electric constant, $\mathbf{n}(t) = \mathbf{R} - \mathbf{r}(t) / \|\mathbf{R} - \mathbf{r}(t)\|$ is the unit vector pointing from the particle to the observation point \mathbf{R} ; $\mathbf{r}(t)$ is the electron trajectory of the reference electron and the dot denotes the time derivative.

The cross spectral density obeys the Wolf equation:

$$[\nabla_j^2 + k^2 n^2(\mathbf{r}_j)] W(\mathbf{r}_1, \mathbf{r}_2, \omega) = 0, \quad (3)$$

where $j = 1, 2$; k is the wave number in free-space, and $n(\mathbf{r})$ is the refractive index. The Wolf equation resembles the Helmholtz equation. Indeed, it can be seen as a tensor product version of the Helmholtz equation. With the Helmholtz equation, the usual Green’s function method for the propagation of wave fields can be derived [3]:

$$E'(\mathbf{r}, \omega) = \frac{1}{2\pi} \int_{\mathcal{A}} d\mathbf{r}' E(\mathbf{r}', \omega) \frac{\partial}{\partial n'} G(\mathbf{r}, \mathbf{r}'), \quad (4)$$

where \mathcal{A} is a closed surface on which E is known, \mathbf{n} is a unit vector normal to \mathcal{A} , and G is a Dirichlet Green’s

function for the wave equation that satisfies appropriate boundary conditions. In consequence, the propagation formula for the cross spectral density takes the form of a tensor product version of the propagation formula of wave fields:

$$W'(\mathbf{r}_1, \mathbf{r}_2, \omega) = \frac{1}{(2\pi)^2} \int_{\mathcal{A}} d\mathbf{r}'_1 \int_{\mathcal{A}} d\mathbf{r}'_2 \times \quad (5)$$

$$W(\mathbf{r}'_1, \mathbf{r}'_2, \omega) \frac{\partial}{\partial n'_1} G^*(\mathbf{r}_1, \mathbf{r}'_1) \frac{\partial}{\partial n'_2} G(\mathbf{r}_2, \mathbf{r}'_2),$$

where \mathbf{n}_1 and \mathbf{n}_2 are unit vectors normal to \mathcal{A} . The spectral density $S(\mathbf{r}, \omega) = W(\mathbf{r}, \mathbf{r}, \omega)$ can be seen as the energy per unit time [4]. The spectral degree of coherence is defined by [5]:

$$\mu(\mathbf{r}_1, \mathbf{r}_2, \omega) = \frac{W(\mathbf{r}_1, \mathbf{r}_2, \omega)}{\sqrt{S(\mathbf{r}_1, \omega)S(\mathbf{r}_2, \omega)}}. \quad (6)$$

The cross spectral density can be represented in terms of eigenvalues $\lambda_m(\omega)$ and coherent modes $\phi_m(\mathbf{r}, \omega)$ [5]:

$$W(\mathbf{r}_1, \mathbf{r}_2, \omega) = \sum_m \lambda_m(\omega) \phi_m^*(\mathbf{r}_1, \omega) \phi_m(\mathbf{r}_2, \omega). \quad (7)$$

The eigenvalues and the coherent modes are the solution of the homogeneous Fredholm integral equation of second kind:

$$\int d\mathbf{r}_1 W(\mathbf{r}_1, \mathbf{r}_2, \omega) \phi_m(\mathbf{r}_1, \omega) = \lambda_m(\omega) \phi_m(\mathbf{r}_2, \omega). \quad (8)$$

This is an eigenvalue problem and may be rewritten as:

$$A_W[\phi_m] = \lambda_m \phi_m \quad (9)$$

with the Hermitian integral operator A_W :

$$A_W[f](\mathbf{r}) = \int d\mathbf{r}' W(\mathbf{r}', \mathbf{r}, \omega) f(\mathbf{r}'). \quad (10)$$

Without loss of generality, the coherent modes can be assumed to be orthonormal. The sum of the eigenvalues equals the integrated spectral density. We will use the notion used in the mathematical field of spectral theory and call the set of the eigenvalues the eigenvalue spectrum. We define the mode distribution as:

$$d_m = \frac{\lambda_m}{\sum_n \lambda_n}. \quad (11)$$

The index $m = 0$ refers to the first coherent mode.

The coherent modes are statistically uncorrelated [5]. The eigenvalue of a coherent mode can therefore be seen as the spectral density carried by this mode and the propagation of the cross spectral density can equally be expressed in terms of propagated coherent modes. Let ϕ'_m denote the propagated coherent mode as if it was an electric field. The propagated cross spectral density W' may be written as:

$$W'(\mathbf{r}_1, \mathbf{r}_2, \omega) = \sum_m \lambda_m(\omega) (\phi'_m(\mathbf{r}_1, \omega))^* \phi'_m(\mathbf{r}_2, \omega). \quad (12)$$

If the eigenvalue spectrum is narrow the propagation of the cross spectral density by means of the propagation of the coherent modes is computationally advantageous. Assume there are N_m coherent modes and the sum of their eigenvalues approximate to a given level of accuracy (e.g. 99%) the total spectral density. Imagine the surface \mathcal{A} in equation Eq. 5 is spanned numerically by a grid of N_{grid} points. If $N_m \ll N_{grid}$ then it is more favorable to calculate Eq. 4 for N_m modes than to calculate Eq. 5.

A prominent model in statistical optics with known analytical coherent mode decomposition is the Gaussian Schell-model (GSM). It is used to model laser modes at the waist [6]. It has been applied to approximate undulator radiation in high emittance storage rings [7-9]. The GSM supposes that the cross spectral density takes a Gaussian form defined by $\sigma_{sx}(\omega)$ and $\sigma_{gx}(\omega)$, the standard deviations of the spectral density and the spectral degree of coherence, respectively. The interest of the model, in addition to its applicability to describe laser radiation, resides in the fact that its decomposition in coherent modes can be done analytically [10, 11] leading to the Gaussian-Hermite eigenfunctions, with eigenvalues that decrease exponentially, as described in the supplementary material. The electric field emitted by the single electron in an undulator is rather complex and in general a Gaussian approximation is not justified. Significant deviations of the cross spectral density from a GSM will become apparent when the electron beam emittance becomes comparable or smaller than the extent of the single electron radiation at the virtual source because radiation details are no longer smeared out by the electron beam. This situation is expected in the case of the new ultra low emittance storage rings.

The electric field of the reference electron E_0 can be calculated only approximately with rather complicated analytical formulas [2, 12] (usually only valid for photon energies close to a harmonic) that lead to integral expressions for which no closed solutions are known. In consequence Eq. 1 can not be solved in a closed form and numerical techniques must be applied.

The innovative aspect of this letter is the successful numerical realisation of a coherent mode decomposition for undulator storage ring emission, i.e. a numerical solution of Eq. 8. The reference electric field E_0 is calculated by numerical integration of Eq. 2 using SRW [13]. We solve the Fredholm equation Eq. 8 numerically with no further approximation using a basis set consisting of normalized two-dimensional step-functions. A two-dimensional step-function is a function that is constant on a rectangle and zero elsewhere. Hereby the center of the rectangle lies on a grid point. The grids we use have constant step width in each direction so our step-functions come from the same mother step-function shifted to cover all the domain without overlapping. The representing matrix of A_W in that basis scales with $N_x^2 N_y^2 = N_{grid}^2$ where N_x, N_y are the numbers of horizontal and vertical grid

points, respectively. This scaling behavior of the representing matrix leads quickly to practically problematic memory requirements. We solve the eigenvalue equation with the iterative eigensolver SLEPc [14]. The library SLEPc allows the implementation of user-defined matrix-vector multiplications that are then used by the eigensolver. We assume an electron phase space density that separates into a spatial part ρ_r , a divergence part ρ_θ and an energy part ρ_γ :

$$A_W(f)(\mathbf{r}_2) = \int d\gamma \rho_\gamma(\gamma) \int d\mathbf{r}_1 d\boldsymbol{\theta} \rho_\theta(\boldsymbol{\theta}) e^{ik\boldsymbol{\theta}(\mathbf{r}_2 - \mathbf{r}_1)} \times \int d\mathbf{r} \rho_r(\mathbf{r}, \gamma) E_0^*(\gamma, \mathbf{r}_1 - \mathbf{r}, \omega) E_0(\gamma, \mathbf{r}_2 - \mathbf{r}, \omega) f(\mathbf{r}_1). \quad (13)$$

The last integral can be considered as an undulator CSD from Eq. 1 with a delta shaped divergence and a fixed electron energy. It can therefore be decomposed into eigenvalues α_n and coherent modes Ψ . The $\boldsymbol{\theta}$ integration can be performed because it is a Fourier transform. The operator A_W can now be rewritten as:

$$A_W(f)(\mathbf{r}_2) = \int d\gamma \rho_\gamma(\gamma) \int d\mathbf{r}_1 \hat{\rho}_\theta(k(\mathbf{r}_2 - \mathbf{r}_1)) \times \sum_n \alpha_n \Psi_n^*(\mathbf{r}_1) \Psi_n(\mathbf{r}_2) f(\mathbf{r}_1). \quad (14)$$

For a few hundreds modes N_m this two-step approach can be performed efficiently numerically. This approach can be easily generalized for electron phase space densities that have an additional spatial and divergence coupling term of the form $e^{C\mathbf{r}\boldsymbol{\theta}}$ where C is a constant. These coupling terms appear if the Twiss alpha value is non zero, i.e. at positions of the lattice that are not a symmetry point. In many cases the memory consumption of the two-step approach is of the order of $N_m \cdot N_{grid}$ while the full representing matrix in the chosen basis set needs N_{grid}^2 elements. The GSM approximation motivates the expectation of a small number of coherent modes for very low emittance storage rings. The number of significant coherent modes depends strongly on the emittance of the lattice and the energy of the undulator radiation. Typical values for N_m are a few hundreds to a few thousands and typical values for N_{grid} are a few hundred thousand.

The coherent modes can be propagated in free space using standard wave optics Fresnel propagation methods. The Gauss-Hermite modes in the Gaussian Schell-model, are invariant under propagation in the far field (Fraunhofer). The coherent modes obtained for undulator radiation do not present, in general, this property. We use SRW for the propagation of the modes. The propagated cross spectral density W' is easily deduced from the propagated modes using Eq. 12. The coherent modes change by propagation in free space, but the eigenvalue spectrum remains constant. An interesting case is the effect of a slit, pinhole, or a more general optical element. When the element cuts the beam (removes intensity), the

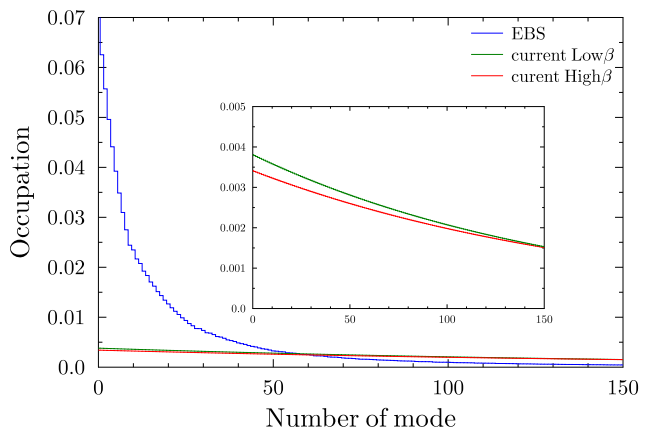


FIG. 1: Eigenvalue spectra for the 2 m long ESRF u18 undulator at its first harmonic for the new ESRF-EBS lattice and for the current ESRF lattice (high and low beta sections). A detailed view of the spectra for the current ESRF lattice is the inset.

eigenfunctions are clipped by a window, so their norm becomes smaller than one. Therefore, the coherent modes and the spectrum of coherent modes of W' are different from those of W and we can solve Eq. 8 again to determine the new coherent modes and eigenvalue spectrum of W' .

Many tests were performed to verify our algorithm. They include delta shaped electron beams, a comparison of the numerical decomposition with a Gaussian reference electric field against the analytical result and comparison to some results that can be calculated by other codes.

We performed a decomposition of the radiation from the 2 m long u18 ESRF undulator for its first harmonic ($E = 7982$ eV, deflection parameter $K = 1.68$) at its virtual source position placed in the current ESRF lattice and in the future ESRF-EBS lattice (parameters from [15] summarized in the supplementary material).

The eigenvalue spectrum (Fig. 1) or mode distribution gives direct information on how the beam spectral density splits into different modes. The m -th mode eigenvalue has an occupation d_m defined by Eq. 11. The occupation of the zeroth mode can be used to define a coherent fraction ($CF = d_0$). In the limit $d_0 \gg d_1$ most of the spectral density is due to the first coherent mode and the contributions of higher coherent modes to the spectral density can be considered as statistical noise. We find that in the case of the ESRF-EBS the coherent fraction is an order of magnitude higher than for the current ESRF lattice (Fig. 1).

Let us now discuss the effect of the electron beam energy spread on the mode spectrum. We use ESRF-EBS lattice settings and an ESRF u18 undulator of 4 m length at its first harmonic. The ESRF-EBS energy spread is

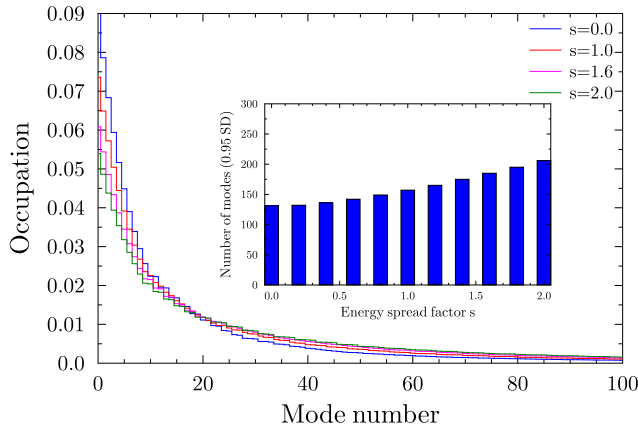


FIG. 2: Number of modes for a few s values of a 95% of the spectral density and the mode distribution (inset) for a linear variation of the energy spread $(\sigma_\delta)' = \sigma_\delta \cdot s$ with a 4m long ESRF u18 undulator and ESRF-EBS lattice settings ($s = 1.0$ corresponds to energy spread of 0.001).

varied according to:

$$(\sigma_\delta)' = \sigma_\delta \cdot s, \quad (15)$$

with $s \in \{0.0, 0.2, 0.4, \dots, 1.0, \dots, 1.8, 2.0\}$, whereas the transverse beam parameters are kept fixed. The energy integration was performed with 27 points. We observe that the total number of coherent modes to incorporate 95% of the spectral density are relatively largely changed (see Fig. 2). The minimal number of coherent modes is 131 which is achieved in the limit of vanishing energy spread. Doubling the ESRF-EBS energy spread results in 206 coherent modes. This is about 30% more than the 157 modes for the present ESRF-EBS lattice settings.

Our implementation of the algorithm can take energy spread into account and works both at positions with zero Twiss alpha (symmetry point), and at positions with finite Twiss alpha as long as the vertical, horizontal and energy dimensions of the electron beam are uncoupled.

We calculated an ideal 1:1 imaging beamline (Fig. 3) at ESRF-EBS lattice settings. A slit S_1 collects the radiation from the undulator and is opened to accept the full central cone. A focusing system is idealized by an ideal lens focusing the virtual source (at 36 m upstream the lens) into the S_2 plane (at 36 m downstream the lens). The decomposition of the radiation in coherent modes at S_1 presents the same spectrum shown before Fig. 1. The spectrum calculated at S_2 is the same as the spectrum in S_1 , because the lens is an ideal element that modifies the individual eigenfunctions but conserves the integral of the spectral density. The CSD can be calculated from the coherent modes. It is a function of four coordinates. We plot horizontal and vertical cuts in Fig. 4. The full-width at half maximum of the profile with one coordinate fixed at zero gives the coherence length of $52.9 \mu\text{m}$ in the

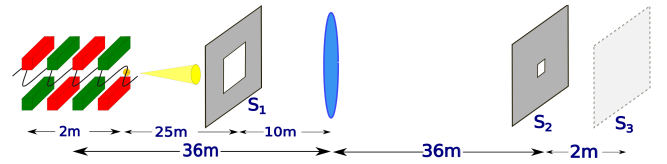


FIG. 3: Schematic view of the 1:1 imaging beamline of the undulator center.

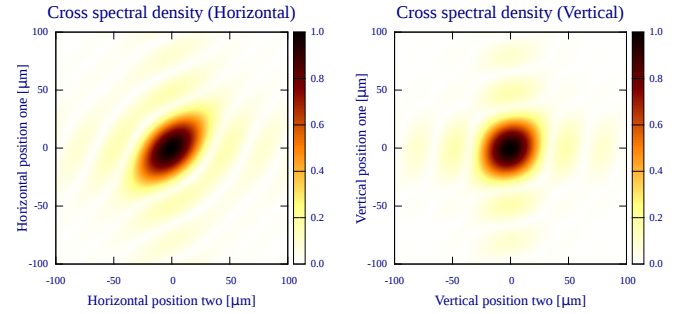


FIG. 4: Vertical and horizontal cuts, i.e. the coordinates of the other dimension are fixed at zero, of the normalized cross spectral density with slit size $5\mu\text{m} \times 5\mu\text{m}$ at S_2 calculated from coherent modes for a 2m long ESRF u18 undulator at the ESRF-EBS lattice at S_3 for the beamline shown in Fig. 3.

horizontal and of $62.4 \mu\text{m}$ the vertical. In the supplementary material these CSD results for a different beamline are compared with SRW Monte-Carlo calculations showing a very good agreement. The first two coherent modes are shown in Fig. 5.

To mimic in an idealized fashion the experiment made in [16] we have at the S_2 plane an aperture with varying size. After the slit aperture we propagate by an addi-

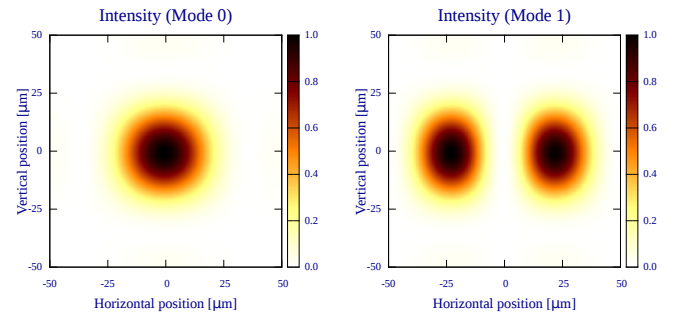


FIG. 5: Zeroth and first coherent modes at S_3 for the beamline shown in Fig. 3 with a $5\mu\text{m} \times 5\mu\text{m}$ aperture size at S_2

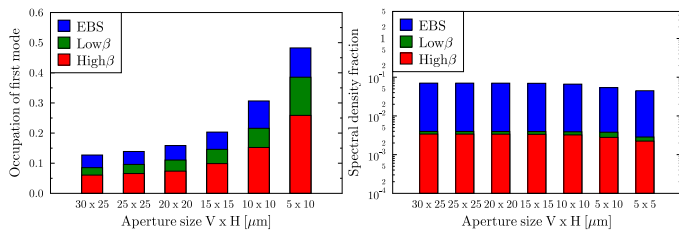


FIG. 6: First mode occupation (left) and spectral density fraction(right) of the first mode at S_3 for a given slit size ($V \times H$ in μm) at S_2 for the beamline shown in Fig. 3. The fraction is calculated with respect to the spectral density at the undulator virtual source.

tional 2 m in free space to the new final position S_3 . At the final position we perform another coherent mode decomposition. We find that reducing the aperture size leads to a narrowing of the eigenvalue spectrum with a simultaneous decrease of spectral density at the final position Fig. 6. We observe that closing the slit improves the overall coherence for the price of spectral density. In the limit $d_0 \gg d_1$ almost the entire spectral density is carried by the first coherent mode. The other modes may be regarded as statistical noise.

In summary we present an algorithm for the numerical coherent mode decomposition for storage ring undulator cross spectral densities. Our implementation of this algorithm can calculate the cross spectral density for positions where the horizontal, vertical and electron energy dimensions of the electron beam are uncoupled. The effect of energy spread and finite Twiss alpha can be taken into account. The eigenvalue spectrum allows to define a quality measure of coherence if the eigenvalue spectrum is dominated by the first coherent mode. We propose a coherence fraction CF as the fraction of the largest eigenvalue over the integrated spectral density. For low emittance storage ring emission, the number of coherent modes is small and we may propagate the cross spectral density to any point in the beamline efficiently by the propagation of the coherent modes. Any simulation that can model the propagation of a single electron emission along the beamline can also be used for the propagation of the coherent modes and then to build the cross spectral density. Additionally to the applications discussed in this paper, the coherent modes could serve as an initial guess for reconstruction algorithms in coherent diffraction imaging techniques. Furthermore, it can be used for modeling X-ray-sample interactions: the coherent modes can be propagated up to the sample position; the action of the sample is applied directly to the propagated modes. This is more efficient than a multi-electron Monte Carlo approach because the optical elements before the sample do not need to be recalculated and the number of coher-

ent modes is in general much smaller than the number of simulated electrons in the Monte Carlo simulation. The same applies to the design of beamlines, where after every design change only a small number of coherent modes after the last modified optical element have to be propagated. The code of our algorithm is open-source and can be found at [17].

-
- [1] K.-J. Kim, “A new formulation of synchrotron radiation optics using the wigner distribution,” *Proc. SPIE 0582, Insertion Devices for Synchrotron Sources*, 2, 1986.
 - [2] G. Geloni, E. Saldin, E. Schneidmiller, and M. Yurkov, “Transverse coherence properties of x-ray beams in third-generation synchrotron radiation sources,” *Nucl. Instrum. Methods A*, 2008.
 - [3] J. Jackson, *Classical electrodynamics*. Wiley, 1975.
 - [4] B. Saleh and M. Teich, *Fundamentals of Photonics*. Wiley Series in Pure and Applied Optics, Wiley, 2007.
 - [5] L. Mandel and E. Wolf, *Optical Coherence and Quantum Optics*. Cambridge University Press, 1995.
 - [6] A. Siegman, *An introduction to lasers and masers*. McGraw-Hill series in the fundamentals of electronic science, McGraw-Hill, 1971.
 - [7] R. Coisson and S. Marchesini, “Gauss–Schell Sources as Models for Synchrotron Radiation,” *J. Synchrotron Radiat.*, vol. 4, pp. 263–266, Sep 1997.
 - [8] I. A. Vartanyants and A. Singer, “Coherence properties of hard x-ray synchrotron sources and x-ray free-electron lasers,” *New Journal of Physics*, vol. 12, p. 035004, 2010.
 - [9] R. R. Lindberg and K.-J. Kim, “Compact representations of partially coherent undulator radiation suitable for wave propagation,” *Phys. Rev. ST Accel. Beams*, vol. 18, p. 090702, Sep 2015.
 - [10] A. Starikov and E. Wolf, “Coherent-mode representation of gaussian schell-model sources and of their radiation fields,” *J. Opt. Soc. Am.*, vol. 72, pp. 923–928, Jul 1982.
 - [11] F. Gori, “Collett-wolf sources and multimode lasers,” *Optics Communications*, vol. 34, no. 3, pp. 301 – 305, 1980.
 - [12] H. Onuki and P. Elleaume, *Undulators, Wigglers and Their Applications*. CRC Press, 2003.
 - [13] O. Chubar and P. Elleaume, “Accurate and efficient computation of synchrotron radiation in the near field region,” *proc. of the EPAC98 Conference*, pp. 1177–1179, 1998.
 - [14] V. Hernandez, J. E. Roman, and V. Vidal, “SLEPC: A scalable and flexible toolkit for the solution of eigenvalue problems,” *ACM Trans. Math. Software*, vol. 31, no. 3, pp. 351–362, 2005.
 - [15] R. Dimper, H. Reichert, P. Raimondi, L. Sanchez Ortiz, F. Sette, and J. Susini, *ESRF Upgrade programme phase II*. ESRF, 2014.
 - [16] P. M. Pelz, M. Guizar-Sicairos, P. Thibault, I. Johnson, M. Holler, and A. Menzel, “On-the-fly scans for x-ray ptychography,” *Appl. Phys. Lett.*, vol. 105, no. 25, 2014.
 - [17] M. Glass, “Comsyl.” <https://www.github.com/mark-glass/comsyl>.